
IMPROVING TIME SERIES CLASSIFICATION ALGORITHMS USING OCTAVE-CONVOLUTIONAL LAYERS

A PREPRINT

Samuel Harford

Department of Mechanical & Industrial Engineering
University of Illinois at Chicago
sharfo2@uic.edu

Fazle Karim

Department of Mechanical & Industrial Engineering
University of Illinois at Chicago
karim1@uic.edu

Houshang Darabi

Department of Mechanical & Industrial Engineering
University of Illinois at Chicago
hdarabi@uic.edu

ABSTRACT

Deep learning models utilizing convolution layers have achieved state-of-the-art performance on univariate time series classification tasks. In this work, we propose improving CNN based time series classifiers by utilizing Octave Convolutions (OctConv) to outperform themselves. These network architectures include Fully Convolutional Networks (FCN), Residual Neural Networks (ResNets), LSTM-Fully Convolutional Networks (LSTM-FCN), and Attention LSTM-Fully Convolutional Networks (ALSTM-FCN). The proposed layers significantly improve each of these models with minimally increased network parameters. In this paper, we experimentally show that by substituting convolutions with OctConv, we significantly improve accuracy for time series classification tasks for most of the benchmark datasets. In addition, the updated ALSTM-OctFCN performs statistically the same as the top two time series classifiers, TS-CHIEF and HIVE-COTE (both ensemble models). To further explore the impact of the OctConv layers, we perform ablation tests of the augmented model compared to their base model.

Keywords Time Series · Classification · Octave Convolution

1 Introduction

Time series data is ubiquitous. It exists in weather readings Taylor et al. [2009], financial recordings Tsay [2005], industrial observations Alwan and Roberts [1988], and psychological signals Jebb et al. [2015], Kadous et al. [2002]. Over the past two decades, classifying these time series data has received enormous attention, and their models are constantly improving. The main objectives of these time series classification algorithms are to perform accurately and efficiently Sharabiani et al. [2018].

Several models have been proposed to classify time series data accurately. Typically, these models are feature-based, ensembles, or deep learning models. Some promising feature-based univariate time series classification models are Bag-of-Words (BoW) Lin et al. [2007], Bag-of-features (TSBF) Baydogan et al. [2013], Bag-of-SFA-Symbols (BOSS) Schäfer [2015], BOSSVS Schäfer [2016], and Word ExtrAction for time Series cLassification (WEASEL) Schäfer and Leser [2017]. In 2007, Lin et al. propose representing time series data using a symbolic representation, which is fed into a BoW classifier Lin et al. [2007]. Subsequently, Baydogan et al. propose utilizing multiple subsequences of random lengths to capture local information of time series data (TSBF) Baydogan et al. [2013]. These subsequences act as a cookbook to classify time series data. In 2015 and 2016, Schäfer et al. proposed BOSS Schäfer [2015] and BOSSVS Schäfer [2016] representing time series data symbolically utilizing histograms and a symbolic Fourier approximation. BOSSVS is an extension of BOSS that reduces the time complexity by utilizing a vector space model. In 2017,

Schafer and Leser proposed WEASEL Schäfer and Leser [2017], an accurate and scalable time series classification model. WEASEL extracts important features by applying a chi-square test on discriminative words that are obtained through a symbolic Fourier approximation. Fast logistic regression utilizes these features to classify time series data. Around the same time, Flynn et al. present RISE, which extracts features of a time series in the time domain (using autocorrelation function, partial autocorrelation function, and an autoregressive model) and features from the frequency domain using power spectrum Flynn et al. [2019]. A random forest is trained on these extracted features to classify the time series data. Nguyen et al. propose utilizing multiple resolutions of symbolic representations, multiple domains representations, and efficient navigation of a huge symbolic word space via a modified symbolic sequence classifier to achieve state-of-the-art results.

Several ensemble models, such as Elastic Ensemble (EE) Lines and Bagnall [2015], Shapelet Ensembles (SE) Bagnall et al. [2015], Flat Collective of Transformation-Based Ensembles (FLAT-COTE) Bagnall et al. [2015], Hierarchical Vote COTE (HIVE-COTE) Lines et al. [2016], and Time Series Combination of Heterogeneous and Integrated Embeddings Shifaz et al. [2020] and have yielded state-of-the-art performance. EE integrates 11 1-NN algorithms via a weighted ensemble method. SE integrates a heterogeneous ensemble on a transformed shapelet. FLAT-COTE. FLAT-COTE combines 35 various time series classifiers into a single classifier by applying a weighted majority vote. HIVE-COTE extends FLAT-COTE by integrating the BOSS and RISE algorithms. More recently, TS-CHIEF Shifaz et al. [2020] utilizes tree-structured classifiers to efficiently ensemble classifiers yielding results similar to HIVE-COTE for a fraction of the time.

Deep learning models have received much attention. Fully Convolutional Network (FCN) Wang et al. [2017], Residual Neural Network (ResNet) Wang et al. [2017], LSTM-FCN, and ALSTM-FCN are currently the state-of-the-art deep learning algorithms for time series classification Karim et al. [2017]. All these algorithms take advantage of convolutional neural network (CNN) layers to extract features to classify univariate time series data. This paper proposes improving all CNN based time series classifiers by substituting the CNN layers with a modified Octave-Convolutional layer. An OctConv layer factorizes the mixed feature maps of a convolutional layer by their frequencies. OctConv has never been applied to time series data or on 1D vectors. Results indicate OctConv to statistically improve the classification accuracy of the various time series deep learning architectures.

The remainder of this paper is structured as follows: Section 2 provides background on univariate time series classifiers and neural network architectures. Section 3 details the proposed methods for this work. Section 4 presents the experiments and results of our proposed methodology on the benchmark univariate time series classifiers. Section 5 concludes the paper and discusses future work.

2 Literature Review

2.1 Fully Convolutional Network

FCNs have proven to be effective deep learning classifiers in many domains including computer vision Wang et al. [2015] and natural language processing Tachibana et al. [2018]. Wang et al. introduced the use of FCNs as a good base for a deep learning based time series classifier Wang et al. [2017]. The input block accepts a univariate time series. This is then passed to three convolutional blocks where each block has a 1-D convolutional layer, followed by batch normalization, and finally a ReLU activation. The convolutional layers have filter sizes of $\{128, 256, 128\}$ and kernel sizes of $\{8, 5, 3\}$, respectively. The convolutional blocks are followed by a global average pooling layer and finally a softmax layer to output a class probability vector.

2.2 Residual Neural Network

ResNets utilize deeper structures of networks and employ skip connections to utilize information from bottom level gradients. ResNets are often utilized in object detection Jung et al. [2017]. Wang et al. explore the use of ResNets for time series classification Wang et al. [2017]. The input block accepts a univariate time series. This is then passed to three residual blocks. Each residual block goes through a 1-D convolutional layer, batch normalization, and ReLU layer three times. The final ReLU layer of each residual block has a skip connection to the input of the block. The filter size for convolutional layers in the same block is the same where the sizes are $\{64, 128, 128\}$ for the respective residual blocks. The three residual blocks are then followed by a global average pooling layer and a softmax output.

2.3 LSTM-FCN & ALSTM-FCN

The LSTM-FCN architecture aims to extract feature information by branching the input Karim et al. [2017]. The input block accepts a univariate time series. The input is then fed to two branches. One branch is an FCN with the same

parameters defined in Section 2.1. The other branch performs a dimension shuffle on the input. This step transposes the input shape from a univariate time series to a multivariate time series where each channel is a single time step. Without the dimension shuffle the model training results in severe overfitting. This branch then passes to an LSTM layer or Attention LSTM layer Bahdanau et al. [2016]. The final step of this branch is a dropout layer. The result of the two branches is then concatenated and fed to a softmax output layer.

2.4 Octave Convolution Layer

The Octave Convolution is formulated as a replacement for general convolutional layers that reduces the spatial redundancy and computational cost Chen et al. [2019]. An OctConv operation consists of decomposing the input into a high and low frequency. Let the high and low frequency output of the OctConv be represented by $Y = \{Y^H, Y^L\}$ where the frequency components are calculated as:

$$\begin{aligned} Y^H &= Y^{H \rightarrow H} + Y^{L \rightarrow H} \\ Y^L &= Y^{L \rightarrow L} + Y^{H \rightarrow L} \end{aligned}$$

where $Y^{H \rightarrow H}$ and $Y^{L \rightarrow L}$ represent the intra-frequency updates, and $Y^{L \rightarrow H}$ and $Y^{H \rightarrow L}$ are the inter-frequency communications. The intra-frequency component is used to update the information within each frequency, while inter-frequency communication further enables information exchange between frequencies.

These intra and inter frequencies can be calculated using the convolutional kernel W and input tensor X . The representation of W is separated into high and low components $W = \{W^H, W^L\}$ responsible for convolving with the respective input component $X = \{X^H, X^L\}$. Each of these components can further be divided into the intra and inter frequencies $W^H = \{W^{H \rightarrow H}, W^{H \rightarrow L}\}$ and $W^L = \{W^{L \rightarrow H}, W^{L \rightarrow L}\}$. This breakdown of components formalize the output tensor calculations as:

$$\begin{aligned} Y_{p,q}^H &= Y^{H \rightarrow H} + Y^{L \rightarrow H} \\ &= \sum_{i,j \in \mathcal{N}_k} W_{i+\frac{k-1}{2}, j+\frac{k-1}{2}}^{H \rightarrow H} \top X_{p+i, q+i}^H \\ &+ \sum_{i,j \in \mathcal{N}_k} W_{i+\frac{k-1}{2}, j+\frac{k-1}{2}}^{L \rightarrow H} \top X_{\lfloor \frac{p}{2} \rfloor + i, \lfloor \frac{q}{2} \rfloor + i}^L \\ Y_{p,q}^L &= Y^{L \rightarrow L} + Y^{H \rightarrow L} \\ &= \sum_{i,j \in \mathcal{N}_k} W_{i+\frac{k-1}{2}, j+\frac{k-1}{2}}^{L \rightarrow L} \top X_{p+i, q+i}^L \\ &+ \sum_{i,j \in \mathcal{N}_k} W_{i+\frac{k-1}{2}, j+\frac{k-1}{2}}^{H \rightarrow L} \top X_{2*p+0.5+i, 2*q+0.5+i}^H \end{aligned}$$

where (p, q) is a location coordinate, $\mathcal{N}_k = \{(i, j) : i = \{-\frac{k-1}{2}, \dots, \frac{k-1}{2}\}, j = \{-\frac{k-1}{2}, \dots, \frac{k-1}{2}\}\}$ is a neighboring coordinate, and $\lfloor \cdot \rfloor$ represents the floor operation. Figure 1 illustrates the interactions of the Octave Convolution.

3 Methodology

3.1 1D Octave Convolutional Layer

Deep learning models have proven to be successful models to classify univariate time series Wang et al. [2017]. The majority of deep learning models for time series classification utilize a series of CNN layers as the primary feature extractor of the neural network architecture. While CNNs have proven to be effective for a variety of deep learning classification tasks, there remains room for improvement in the feature extraction of these layers. In this work, we propose extensions of deep learning models for time series classification with the use of OctConv layers instead of CNN layers. We replace the convolutional layers for Octave Convolutions, OctConv Fully Convolutional Network (OctFCN), OctConv Residual Neural Network (OctResNet), LSTM-OctConv Fully Convolutional Network (LSTM-OctFCN), Attention LSTM-OctConv Fully Convolutional Network and (ALSTM-OctFCN) we use are for the OctConv layer to the case of 1D sequence models to enhance classification accuracies for each model.

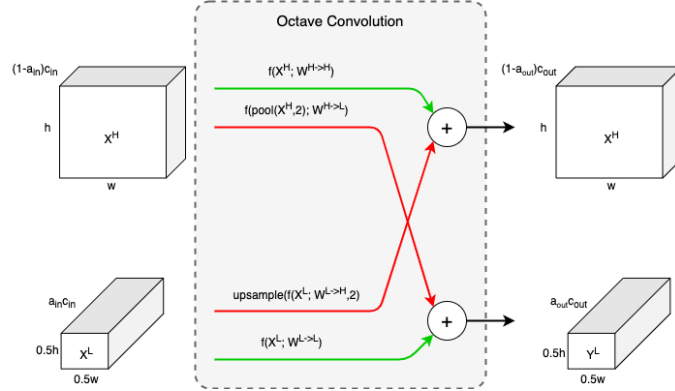


Figure 1: Octave Convolution.

The OctConv augmentation to the models in Figure 2D-F aims to enhance the feature extraction at each layer. The initial OctConv layer takes the same input shape as the original convolutional layer. The filter size f_{init} for the initial layer is split based on a parameter α which is set to 0.5. The high filter is achieved by feeding the input to a 1-D convolutional layer with filter size of $\alpha * f_{init}$. The low filter is achieved by first downsampling the input through a 1D average pool and then fed to a 1-D convolutional layer with filter size of $(1 - \alpha) * f_{init}$. The initial layer then outputs a high and low filter component. The intermediate layers of the OctConv blocks take as input a high and low component and again split each component by the factor α and the filter size f_{inte} . The high \rightarrow high component is obtained through a 1-D convolution of the high input with a filter size of $(1 - \alpha) * f_{inte}$. The low \rightarrow high component is obtained through a 1-D convolution of the low input with a filter size of $(1 - \alpha) * f_{inte}$ and then performing a 1-D upsampling. The final high component is calculated by an elementwise addition of the high \rightarrow high and low \rightarrow high components. The high \rightarrow low component is obtained through a 1-D average pooling of the high input and then fed to a 1-D convolution with a filter size of $\alpha * f_{inte}$. The low \rightarrow low component is obtained through a 1-D convolution of the low input with a filter size of $\alpha * f_{inte}$. The final low component is the elementwise addition of the high \rightarrow low and low \rightarrow low components. The final layer of the OctConv block takes as input a high and low component and the filter size f_{fin} . Both the high and low inputs are fed to 1-D convolutions with filter size f_{fin} . The low component is then upsampled to match shapes. The high and low components are finally added together to can the final OctConv output.

OctConv layers aim to save on computational processing and memory through the use of the high and low filter Chen et al. [2019]. In addition, the processing for features in the high and low filters results in better model performance overall. In this work, we aim to understand the impact of OctConv’s ability to capture global information through the task of time series classification. The Octave Convolution function aims to improve performance over transitional convolutions by exploiting the low- and high-frequency information and increasing the field size to learn better global information.

3.2 Network Architectures

In this section, we describe the model architectures for the four most common CNN based time series classifiers.

3.2.1 OctConv Fully Convolutional Network

The OctFCN architecture is an extension of the FCN introduced in Section 2.1. Figure 2A illustrates the OctFCN architecture. The input block accepts a univariate time series. This is then passed to three OctConv blocks where each block has a 1-D Octave Convolutional layer, followed by batch normalization, and finally a ReLU activation. The 1-D Octave Convolutional layers have filter sizes of $\{128, 256, 128\}$ and kernel sizes of $\{8, 5, 3\}$, respectively. The three OctConv blocks are followed by a global average pooling layer and finally a softmax layer to output a class probability vector.

3.2.2 OctConv Residual Neural Network

The OctResNet architecture is an extension of the ResNet introduced in Section 2.2. Figure 2B illustrates the OctResNet architecture. The input block accepts a univariate time series. This is then passed to three modified residual blocks. Each of these blocks goes through a 1-D Octave Convolutional layer, batch normalization, and ReLU layer three times. The final ReLU layer of each residual block has a skip connection to the input of the block. The filter size for 1-D

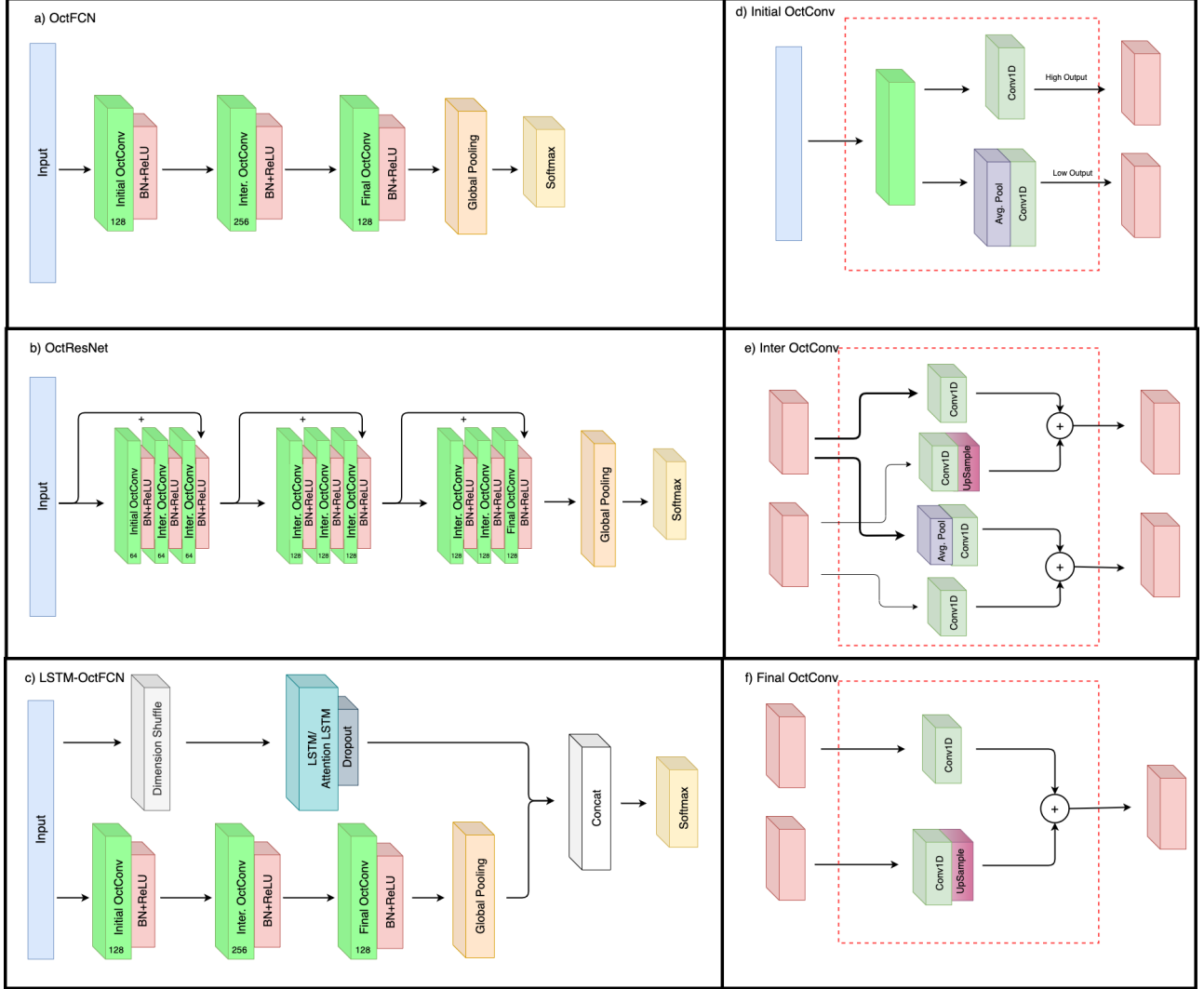


Figure 2: Neural Network Augmentations and OctConv Blocks

Octave Convolutional layers in the same block is the same where the sizes are $\{64, 128, 128\}$ for the respective blocks. The three modified residual blocks are then followed by a global average pooling layer and a softmax output.

3.2.3 A/LSTM-OctConv Fully Convolutional Network

The LSTM-OctFCN architecture is an extension of the LSTM-FCN introduced in Section 2.3. Figure 2C illustrates the LSTM-OctFCN architecture. The input block accepts a univariate time series. The input is then fed to two branches. One branch is an OctFCN with three OctConv blocks where each block has a 1-D Octave Convolutional layer, followed by batch normalization, and finally a ReLU activation. The 1-D Octave Convolutional layers have filter sizes of $\{128, 256, 128\}$ and kernel sizes of $\{8, 5, 3\}$, respectively. The other branch performs a dimension shuffle on the input. This step transposes the input shape from a univariate time series to a multivariate time series where each channel is a single time step. The final step of this branch is a dropout layer. This branch is not modified because there are no CNN layers. The result of the two branches is then concatenated and fed to a softmax output layer.

3.3 Training & Evaluation Methodology

Time series datasets are defined as a tensor of shape (N, Q, M) , where N is the number of samples, Q is the maximum length of a time series, and M is the number of dimensions. In the case of univariate time series M is 1 for all datasets.

While this study focuses on univariate time series classification, the models can easily be extended to multivariate applications.

The primary modeling parameters for each network architecture are defined in Section 3.1. The majority of these parameters are constant for all datasets that are modeling. During the training of the neural networks and their OctConv variants, a gridsearch of optimal parameters is not conducted. The objective of these experiments is to compare the augmentation of the convolution layers, not to obtain the optimal model. The only exception is the number of units in the LSTM for the LSTM-FCN and LSTM-OctFCN models. These units have been optimized in previous works and are utilized in our study Karim et al. [2017, 2019].

In this paper, various models are evaluated using accuracy and rank. To fairly compare these models, we use an average of 20 runs for each model.

4 Experiments & Results

4.1 Univariate Time Series Benchmarks

The current University of California-Riverside (UCR) time series classification benchmark consists of 128 univariate datasets Dau et al. [2019]. The first 85 datasets were introduced in the 2015 version of the benchmarks. These datasets consist of univariate time series with uniform length and z-normalization preprocessing. The additional 43 datasets in the current version aim to address the issues of the data and task the user with more realistic classification benchmarks. This includes the addition of varying length time series and removes the preprocessing of time series benchmarks.

4.2 VS Deep Learning Classifiers

This study aims to show the impact of the OctConv layer as a replacement for a traditional convolutional layer. This replacement is evaluated by comparing neural networks trained using the convolutional layer compared to the same architecture with OctConv in place of the convolutional layers. These neural networks include the FCN, ResNet and LSTM-FCN introduced in Figure 2. In addition, a modified LSTM-FCN for an attention lstm (ALSTM-FCN) is evaluated during the experiments.

To compare a neural network to its OctConv version, the average accuracy of 20 trained networks is used as the final metric for each classifier. The Wilcoxon signed-rank test (WSRT) is a non-parametric statistical test that hypothesizes the median of the rank between the compared models is similar. The alternative hypothesis of the WSRT is that the median of the rank is not similar for compared models. The WSRT is used to evaluate the performance of base neural networks with their OctConv versions. Table 1 shows the results of the WSRT for the four neural networks explored in this study. At a p-value of 0.05 all of the evaluated networks show a significant improvement in accuracy across the benchmark datasets. This shows the impact of the OctConv in place of the traditional convolution results in significantly better models in a variety of neural networks for the task of time series classification.

Table 1: Wilcoxon Signed-Rank Test comparing AVERAGE testing accuracy of Models developed with traditional convolutions vs OctConvs (p-value shown)

Model	Oct P-Value
FCN	4.60E-07
Resnet	3.19E-13
LSTM-FCN	3.51E-10
ALSTM-FCN	1.63E-09

In addition to the average accuracy, the maximum accuracy of 20 trained networks is compared. Table 2 shows the results of the WSRT for the four neural networks based on the maximum accuracy. At a p-value of 0.05 all networks except ALSTM-FCN show to have a significant improvement in maximum accuracy on the benchmark datasets.

Figure 3 illustrates a critical difference diagram for the models evaluated in this study. The critical difference diagram is conducted using a Wilcoxon-Holm post-hoc analysis to evaluate the arithmetic means of the ranks Fawaz et al. [2019]. This figure confirms that each neural network has a lower rank than that of its original version.

4.3 VS State-of-the-Art Classifiers

As an additional evaluation, we compare our results to those reported as existing non-deep learning state-of-the-art (SOTA) models. These include models such as TS-CHIEF Shifaz et al. [2020], ROCKET Dempster et al. [2020],

Table 2: Wilcoxon Signed-Rank Test comparing MAXIMUM testing accuracy of Models developed with traditional convolutions vs OctConvs (p-value shown)

Model	Oct P-Value
FCN	7.44E-05
Resnet	1.33E-03
LSTM-FCN	9.21E-04
ALSTM-FCN	5.22E-02

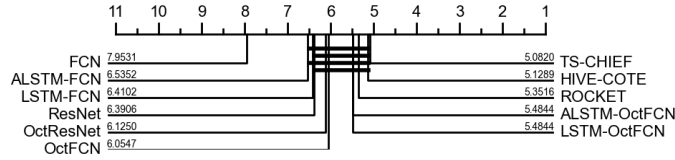


Figure 3: Critical difference diagram of the arithmetic means of the ranks for Deep Learning Models

HIVE-COTE Lines et al. [2018] and more. As stated in Section 3.3, our model accuracies are evaluated on an average of 20 runs. For existing models, we utilize the metrics reported in the literature.

Table 5 shows the results for the models developed in this study compared to the existing SOTA models for time series classification on the 128 benchmark datasets. The first 85 datasets are from the original achieve. These datasets have been available for research and compared more rigorously than the new datasets. For this reason, the SOTA models are more easily available for comparison through the existing literature. The remainder shows the SOTA for the remaining 43 benchmark datasets. Bold cells in these tables indicate the developed models that achieve higher accuracy than the existing SOTA.

Figure 3 illustrates the critical difference diagram of our models and the top SOTA models. These SOTA models often rely on ensemble techniques to boost optimal performance. The purpose of this study is not to statistically outperform SOTA models on the benchmark, rather to illustrate the effectiveness of the OctConv layer in the place of convolutional layers. Table 3 shows the results of the WSRT for the four OctConv neural networks compared to TS-CHIEF, ROCKET, and HIVE-COTE. At a significance level of 0.05, both OctResNet and LSTM-OctFCN is outperformed by HIVE-COTE, TS-CHIEF, and ROCKET. Oct-FCN performs statistically the same as TS-CHIEF. Interestingly, ALSTM-FCN performs statistically the same as the top 2 time series classifiers, HIVE-COTE and TS-CHIEF. This result shows that a simple update of a convolution layer to an octave convolution layer, not only improves its own performance, but leads ALSTM-OctFCN to perform similarly to top two SOTA TSC classifiers (HIVE-COTE and TS-CHIEF).

4.4 Ablation

As an additional evaluation for the impact of the OctConv layer, an ablation study is conducted to show the impact of the replacement for feature extraction. Figure 5 shows the differences in input transformation of FCN and OctFCN for a single input of the CBF dataset. These visuals depict randomly selected filters for each of the models. Both models show clear learned feature extraction in the series of layers, however the two models result in very different noise reduction steps. While these visuals clearly show the superior feature extraction of the OctConv layers, we further study the outcomes through the use of a linear kernel classifier.

In order to explicitly determine the impact of these different methods, we evaluate the features from the developed models when applied to an SVM classifier with a linear kernel. For each of the developed models (FCN, ResNet, LSTM-FCN, and ALSTM-FCN) the features are fed to SVM classifiers to get an explicit evaluation of the extracted features. For the LSTM-FCN and ALSTM-FCN models, only the FCN component of the network is analyzed in this ablation study.

Table 4 shows the results of the WSRT comparing the accuracy for an SVM developed with convolutional features vs an SVM developed with OctConv features. These results show that (at a p-value of 0.05) there is a significant improvement of the SVM developed with OctConv features than that of the convolutional features. Based on this analysis, we can conclude that the OctConv is doing a better job creating linearly separable classes than the convolutional layer. We postulate that the OctConv layers are better because the high and low filters do a better job of capturing the global information at each layer.

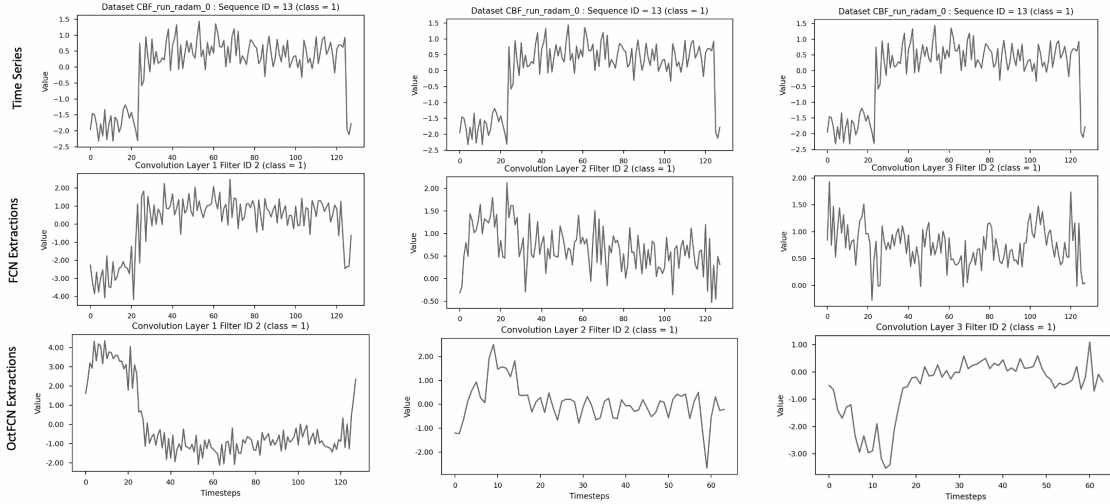


Figure 4: Ablation visual representation of the input signal after transformation in FCN and OctConv through randomly selected filters from each layer

Table 3: Wilcoxon Signed-Rank Test comparing AVERAGE testing accuracy of Models developed with OctConvs to some of the SOTA models (p-value shown)

Model	HIVE-COTE	TS-CHIEF	ROCKET
OctFCN	4.15E-02	9.78E-02	1.06E-02
OctResnet	2.56E-03	1.96E-02	7.37E-04
LSTM-OctFCN	6.31E-04	4.65E-03	9.81E-05
ALSTM-OctFCN	7.20E-02	1.12E-01	1.33E-02

5 Conclusion

In this work, we propose the replacement of traditional convolutional layers with Octave Convolutional layers. We evaluate this replacement on four state-of-the-art neural network architectures including FCN, ResNet, LSTM-FCN, and ALSTM-FCN. The experiments for this study utilize the 128 datasets provided by the University of California-Riverside time series classification archive. These experiments show that on an average of 20 runs on each dataset the tested neural networks perform significantly better when the convolutional layers are replaced with Octave Convolutional layers. Based on the average testing accuracy of 20 runs, ALSTM-OctFCN performs statistically the same as the top two time series classifiers, TS-CHIEF and HIVE-COTE. To further evaluate the replaced layers, we provide an ablation study of the features extracted by each neural network classifier. This ablation study establishes that the features extracted by the Octave Convolutional layers provide better information than that of the traditional convolutional layers. Future research in this area can explore the use of other alternatives to convolutional layers that may outperform the Octave Convolution. In addition, the generated models may be considered in an ensemble model to achieve state-of-the-art performance on the time series classification benchmarks.

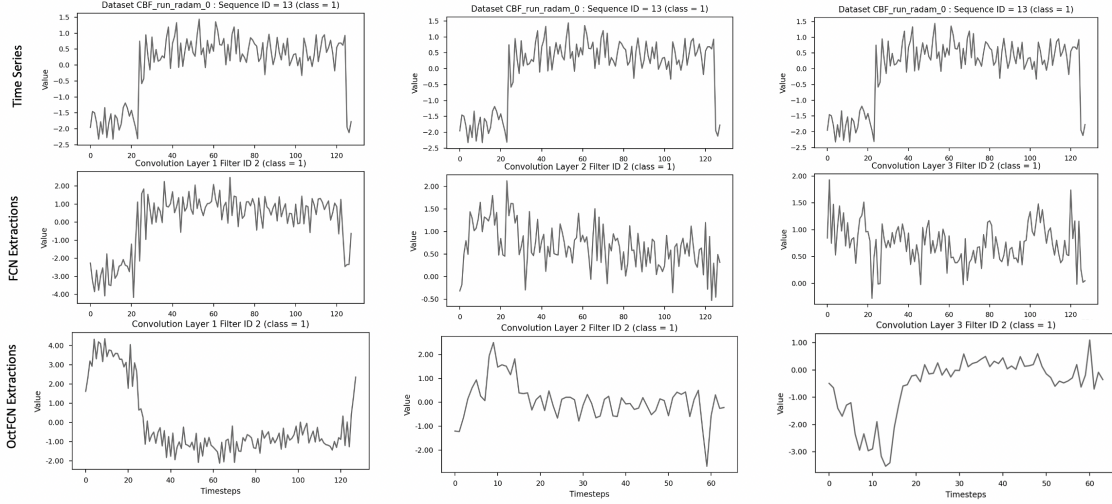


Figure 5: Ablation visual representation of the input signal after transformation in FCN and OctConv through randomly selected filters from each layer

Table 4: Wilcoxon Signed-Rank Test comparing the SVM models developed from traditional convolutions vs OctConvs information (p-value shown)

Model	P-Value
FCN	6.06E-05
Resnet	8.67E-08
LSTM-FCN	1.70E-08
ALSTM-FCN	8.35E-06

Table 5: Classification Accuracy for the Benchmark Datasets

Dataset	FCN	Oct FCN	ResNet	Oct ResNet	LSTM -FCN	LSTM -OctFCN	ALSTM -FCN	ALSTM -OctFCN	SOTA
Adiac	0.768	0.801	0.833	0.828	0.826	0.823	0.811	0.821	0.857
ArrowHead	0.816	0.855	0.813	0.846	0.869	0.884	0.813	0.868	0.880
ChlorineConcentration	0.800	0.800	0.817	0.813	0.800	0.811	0.798	0.807	0.875
InsectWingbeatSound	0.382	0.451	0.448	0.541	0.649	0.654	0.385	0.454	0.653
Lighting7	0.740	0.814	0.703	0.784	0.745	0.775	0.749	0.814	0.863
Wine	0.596	0.778	0.759	0.681	0.672	0.770	0.717	0.756	0.889
WordsSynonyms	0.532	0.607	0.609	0.655	0.657	0.668	0.544	0.608	0.779
50words	0.656	0.694	0.683	0.722	0.781	0.801	0.659	0.696	0.846
Beef	0.747	0.680	0.773	0.757	0.803	0.757	0.763	0.720	0.933
DistPhalOutAgeGroup	0.799	0.799	0.805	0.785	0.823	0.807	0.825	0.816	0.835
DistPhalOutCorrect	0.803	0.800	0.798	0.790	0.803	0.798	0.801	0.794	0.820
DistalPhalanxTW	0.776	0.764	0.766	0.762	0.779	0.767	0.783	0.771	0.790
ECG200	0.876	0.900	0.892	0.907	0.884	0.899	0.891	0.898	0.920
ECGFiveDays	0.989	0.993	0.980	0.991	0.985	0.990	0.986	0.993	1.000
BeetleFly	0.810	0.855	0.850	0.850	0.860	0.900	0.785	0.850	0.950
BirdChicken	0.935	0.915	0.925	0.910	0.900	0.900	0.935	0.910	0.950
ItalyPowerDemand	0.959	0.956	0.961	0.958	0.959	0.956	0.959	0.956	0.970
SonyAIBORobotSur	0.964	0.957	0.916	0.928	0.938	0.934	0.961	0.961	0.985
SonyAIBORobotSurII	0.972	0.965	0.980	0.970	0.972	0.962	0.976	0.966	0.978
MidPhalOutAgeGroup	0.749	0.736	0.751	0.733	0.742	0.737	0.746	0.742	0.814
MidPhalOutCor	0.817	0.798	0.816	0.791	0.814	0.806	0.816	0.800	0.808
MiddlePhalanxTW	0.585	0.605	0.595	0.593	0.595	0.599	0.594	0.593	0.612
ProxPhalOutAgeGroup	0.833	0.835	0.853	0.844	0.845	0.837	0.845	0.835	0.883

ProxPhalOutCorrect	0.902	0.910	0.914	0.908	0.906	0.910	0.906	0.910	0.918
ProximalPhalanxTW	0.811	0.802	0.816	0.791	0.814	0.799	0.810	0.805	0.815
MoteStrain	0.918	0.906	0.909	0.901	0.927	0.908	0.920	0.903	0.950
MedicalImages	0.768	0.753	0.756	0.755	0.768	0.751	0.771	0.760	0.792
Strawberry	0.964	0.965	0.964	0.962	0.963	0.965	0.966	0.966	0.980
ToeSegmentation1	0.975	0.967	0.965	0.964	0.971	0.965	0.970	0.964	0.974
Coffee	1.000	1.000	1.000	1.000	1.000	1.000	1.000	1.000	1.000
Cricket_X	0.773	0.791	0.788	0.814	0.746	0.762	0.782	0.791	0.821
Cricket_Y	0.764	0.798	0.798	0.819	0.759	0.798	0.770	0.795	0.826
Cricket_Z	0.774	0.812	0.804	0.823	0.786	0.809	0.783	0.812	0.836
uWaveGestLib_X	0.757	0.773	0.763	0.782	0.832	0.834	0.766	0.774	0.855
uWaveGestLib_Y	0.649	0.674	0.652	0.682	0.727	0.745	0.668	0.676	0.759
uWaveGestLib_Z	0.737	0.745	0.736	0.747	0.777	0.773	0.740	0.745	0.792
ToeSegmentation2	0.903	0.929	0.899	0.928	0.905	0.933	0.905	0.927	0.962
DiatomSizeReduction	0.940	0.930	0.952	0.933	0.937	0.937	0.937	0.936	0.977
Car	0.913	0.932	0.888	0.907	0.917	0.902	0.915	0.927	0.933
CBF	0.994	0.996	0.995	0.998	0.994	0.996	0.993	0.996	1.000
CinC_ECG_torso	0.832	0.847	0.809	0.843	0.890	0.890	0.830	0.848	0.996
Computers	0.844	0.832	0.814	0.814	0.775	0.734	0.836	0.828	0.848
Earthquakes	0.763	0.793	0.760	0.794	0.794	0.801	0.783	0.797	0.801
ECG5000	0.939	0.941	0.940	0.940	0.942	0.942	0.940	0.941	0.948
ElectricDevices	0.714	0.705	0.722	0.705	0.742	0.732	0.717	0.719	0.799
FaceAll	0.922	0.864	0.848	0.813	0.910	0.875	0.914	0.868	0.929
FaceFour	0.934	0.953	0.950	0.953	0.874	0.876	0.934	0.955	1.000
FacesUCR	0.933	0.952	0.942	0.946	0.917	0.932	0.934	0.951	0.965
Fish	0.937	0.969	0.971	0.983	0.958	0.967	0.953	0.972	0.994
FordA	0.919	0.924	0.921	0.928	0.918	0.931	0.915	0.924	0.973
FordB	0.880	0.902	0.916	0.918	0.883	0.904	0.881	0.902	0.917
Gun_Point	1.000	1.000	0.997	1.000	0.995	0.998	1.000	1.000	1.000
Ham	0.715	0.750	0.712	0.730	0.717	0.727	0.720	0.750	0.781
HandOutlines	0.521	0.755	0.880	0.871	0.842	0.875	0.623	0.806	0.960
Haptics	0.426	0.494	0.517	0.553	0.489	0.514	0.465	0.510	0.551
Herring	0.634	0.703	0.614	0.661	0.641	0.698	0.647	0.727	0.703
InlineSkate	0.374	0.423	0.482	0.432	0.465	0.446	0.424	0.427	0.613
LargeKitApp	0.890	0.895	0.903	0.897	0.685	0.744	0.897	0.897	0.896
Lighting2	0.708	0.711	0.730	0.726	0.752	0.769	0.718	0.728	0.885
MALLAT	0.963	0.966	0.938	0.961	0.963	0.961	0.966	0.966	0.980
Meat	0.863	0.875	0.938	0.942	0.895	0.922	0.885	0.910	1.000
NonInvFatECGThor1	0.949	0.958	0.954	0.955	0.962	0.962	0.955	0.956	0.962
NonInvFatECGThor2	0.929	0.947	0.949	0.956	0.954	0.957	0.948	0.951	0.969
OliveOil	0.533	0.720	0.827	0.847	0.593	0.770	0.587	0.767	0.933
OSULeaf	0.979	0.970	0.974	0.965	0.895	0.907	0.979	0.971	0.988
PhalOutlCor	0.813	0.821	0.825	0.821	0.816	0.817	0.812	0.817	0.854
Phoneme	0.336	0.345	0.354	0.345	0.252	0.265	0.340	0.343	0.349
Plane	1.000	1.000	1.000	1.000	1.000	1.000	1.000	1.000	1.000
RefrigerationDevices	0.510	0.528	0.555	0.534	0.466	0.480	0.507	0.525	0.581
ScreenType	0.637	0.637	0.648	0.627	0.545	0.510	0.639	0.634	0.707
ShapeletSim	0.956	0.926	0.948	0.874	0.966	0.953	0.927	0.921	1.000
ShapesAll	0.885	0.903	0.912	0.917	0.890	0.904	0.884	0.902	0.930
SmallKitApp	0.734	0.759	0.769	0.735	0.610	0.599	0.766	0.757	0.853
StarlightCurves	0.964	0.975	0.976	0.977	0.965	0.974	0.964	0.975	0.982
SwedishLeaf	0.969	0.966	0.960	0.960	0.971	0.968	0.968	0.968	0.966
Symbols	0.973	0.983	0.972	0.980	0.963	0.963	0.976	0.984	0.982
synthetic_control	0.985	0.999	0.994	0.998	0.978	0.999	0.980	0.999	1.000
Trace	0.250	0.250	0.250	0.250	0.250	0.250	0.250	0.250	1.000
Two_Patterns	0.863	0.942	0.963	0.991	0.994	0.984	0.873	0.943	1.000

TwoLeadECG	0.999	0.998	0.999	0.996	0.999	0.998	0.999	0.998	1.000
UWaveGestLibAll	0.822	0.864	0.833	0.874	0.955	0.959	0.824	0.861	0.976
Wafer	0.997	0.999	0.995	0.997	0.998	0.999	0.997	0.998	1.000
Worms	0.612	0.650	0.598	0.626	0.494	0.534	0.606	0.651	0.805
WormsTwoClass	0.773	0.774	0.771	0.762	0.683	0.699	0.781	0.773	0.831
yoga	0.860	0.879	0.878	0.888	0.903	0.904	0.879	0.883	0.918
ACSF1	0.927	0.935	0.917	0.932	0.903	0.920	0.913	0.940	0.850
AllGestWiX	0.615	0.646	0.707	0.718	0.693	0.724	0.718	0.722	0.717
AllGestWiY	0.746	0.778	0.764	0.773	0.753	0.781	0.788	0.856	0.730
AllGestWiZ	0.694	0.725	0.715	0.720	0.704	0.758	0.733	0.746	0.651
BME	0.947	0.980	0.953	0.968	0.952	0.996	0.833	0.900	0.999
Chinatown	0.938	0.956	0.964	0.973	0.988	0.988	0.985	0.995	0.970
Crop	0.764	0.783	0.789	0.793	0.764	0.875	0.762	0.799	0.793
DodgLpDay	0.614	0.647	0.647	0.648	0.634	0.652	0.486	0.550	0.588
DodgLpGm	0.826	0.833	0.846	0.856	0.893	0.907	0.779	0.823	0.928
DodgLpWnd	0.938	0.967	0.949	0.949	0.927	0.933	0.970	0.973	0.986
EOGHZsgn	0.651	0.656	0.652	0.663	0.617	0.632	0.686	0.680	0.884
EOGVtSgn	0.473	0.490	0.465	0.472	0.504	0.529	0.514	0.518	0.815
EthLevel	0.737	0.743	0.753	0.737	0.725	0.763	0.738	0.727	0.875
FrzRegTr	0.957	0.991	0.970	0.965	0.998	1.000	1.000	1.000	0.999
FRSmlTr	0.829	0.842	0.816	0.822	0.807	0.836	0.878	0.897	0.995
Fungi	0.983	0.998	0.994	0.996	0.984	1.000	0.995	1.000	0.839
GestMidAirD1	0.736	0.742	0.719	0.746	0.703	0.751	0.714	0.751	0.639
GestMidAirD2	0.672	0.677	0.657	0.669	0.694	0.681	0.640	0.628	0.608
GestMidAirD3	0.421	0.440	0.390	0.433	0.452	0.433	0.444	0.435	0.377
GestPebZ1	0.944	0.973	0.941	0.949	0.947	0.933	0.921	0.921	0.826
GestPebZ2	0.857	0.883	0.892	0.864	0.873	0.913	0.832	0.818	0.779
GunPtAgeSp	0.982	0.973	0.998	0.995	0.986	0.988	1.000	0.970	1.000
GunPontMVsf	0.962	0.987	0.976	0.957	0.980	0.989	1.000	1.000	1.000
GunPointOVsY	0.942	0.949	0.995	0.957	0.974	0.983	1.000	0.986	1.000
HouseTwenty	0.945	0.955	0.908	0.961	0.970	0.962	0.948	0.970	0.979
InsEPGRegTr	1.000	1.000	1.000	0.995	1.000	0.994	1.000	0.991	1.000
InsEPGSmlTr	0.928	0.958	1.000	0.920	1.000	0.981	1.000	0.976	1.000
MelbPed	0.972	0.993	0.983	0.988	0.973	0.951	0.976	0.979	0.848
MxShpRegTr	0.928	0.942	0.975	0.984	0.963	0.991	0.968	0.981	0.971
MxShpSmlTr	0.918	0.941	0.928	0.936	0.922	0.927	0.924	0.915	0.947
PickGestWiZ	0.853	0.878	0.864	0.851	0.897	0.895	0.899	0.900	0.660
PigAryPress	0.750	0.760	0.753	0.740	0.793	0.824	0.756	0.826	0.977
PigArtPress	0.964	0.974	0.974	0.977	0.985	1.000	0.995	1.000	0.975
PigCVP	0.864	0.869	0.871	0.937	0.922	0.941	0.928	0.956	0.961
PLAID	0.481	0.489	0.482	0.494	0.282	0.483	0.506	0.515	0.840
PowerCons	0.973	0.984	0.973	0.981	1.000	1.000	0.984	1.000	0.993
Rock	0.718	0.727	0.676	0.729	0.764	0.782	0.795	0.805	0.867
SgHdGendCh2	0.943	0.969	0.937	0.959	0.945	0.986	0.852	0.879	0.969
SgHdMovCh2	0.612	0.626	0.698	0.630	0.703	0.714	0.653	0.716	0.891
SgHdSubCh2	0.919	0.927	0.925	0.932	0.917	0.917	0.902	0.917	0.951
ShkGestWiZ	0.961	0.981	0.973	0.966	0.946	0.992	0.975	0.974	0.860
SmthSub	0.986	0.983	0.993	0.988	1.000	0.988	1.000	1.000	0.998
UMB	0.989	1.000	1.000	0.982	1.000	0.966	0.989	1.000	0.983

References

- James W Taylor, Patrick E McSharry, and Roberto Buizza. Wind power density forecasting using ensemble predictions and time series models. *IEEE Transactions on Energy Conversion*, 24(3):775–782, 2009.
- Ruey S Tsay. *Analysis of financial time series*, volume 543. John wiley & sons, 2005.

- Layth C Alwan and Harry V Roberts. Time-series modeling for statistical process control. *Journal of Business & Economic Statistics*, 6(1):87–95, 1988.
- Andrew T Jebb, Louis Tay, Wei Wang, and Qiming Huang. Time series analysis for psychological research: examining and forecasting change. *Frontiers in psychology*, 6:727, 2015.
- Mohammed Waleed Kadous et al. *Temporal classification: Extending the classification paradigm to multivariate time series*. University of New South Wales Kensington, 2002.
- Anooshiravan Sharabiani, Houshang Darabi, Samuel Harford, Elnaz Douzali, Fazle Karim, Hereford Johnson, and Shun Chen. Asymptotic dynamic time warping calculation with utilizing value repetition. *Knowledge and Information Systems*, 57(2):359–388, 2018.
- Jessica Lin, Eamonn Keogh, Li Wei, and Stefano Lonardi. Experiencing sax: a novel symbolic representation of time series. *Data Mining and knowledge discovery*, 15(2):107–144, 2007.
- Mustafa Gokce Baydogan, George Runger, and Eugene Tuv. A bag-of-features framework to classify time series. *IEEE transactions on pattern analysis and machine intelligence*, 35(11):2796–2802, 2013.
- Patrick Schäfer. The boss is concerned with time series classification in the presence of noise. *Data Mining and Knowledge Discovery*, 29(6):1505–1530, 2015.
- Patrick Schäfer. Scalable time series classification. *Data Mining and Knowledge Discovery*, 30(5):1273–1298, 2016.
- Patrick Schäfer and Ulf Leser. Fast and accurate time series classification with weasel. In *Proceedings of the 2017 ACM on Conference on Information and Knowledge Management*, pages 637–646, 2017.
- Michael Flynn, James Large, and Tony Bagnall. The contract random interval spectral ensemble (c-rise): the effect of contracting a classifier on accuracy. In *International Conference on Hybrid Artificial Intelligence Systems*, pages 381–392. Springer, 2019.
- Jason Lines and Anthony Bagnall. Time series classification with ensembles of elastic distance measures. *Data Mining and Knowledge Discovery*, 29(3):565–592, 2015.
- Anthony Bagnall, Jason Lines, Jon Hills, and Aaron Bostrom. Time-series classification with cote: the collective of transformation-based ensembles. *IEEE Transactions on Knowledge and Data Engineering*, 27(9):2522–2535, 2015.
- Jason Lines, Sarah Taylor, and Anthony Bagnall. Hive-cote: The hierarchical vote collective of transformation-based ensembles for time series classification. In *2016 IEEE 16th international conference on data mining (ICDM)*, pages 1041–1046. IEEE, 2016.
- Ahmed Shifaz, Charlotte Pelletier, François Petitjean, and Geoffrey I Webb. Ts-chief: A scalable and accurate forest algorithm for time series classification. *Data Mining and Knowledge Discovery*, pages 1–34, 2020.
- Zhiguang Wang, Weizhong Yan, and Tim Oates. Time series classification from scratch with deep neural networks: A strong baseline. In *2017 International joint conference on neural networks (IJCNN)*, pages 1578–1585. IEEE, 2017.
- Fazle Karim, Somshubra Majumdar, Houshang Darabi, and Shun Chen. Lstm fully convolutional networks for time series classification. *IEEE access*, 6:1662–1669, 2017.
- Lijun Wang, Wanli Ouyang, Xiaogang Wang, and Huchuan Lu. Visual tracking with fully convolutional networks. In *Proceedings of the IEEE international conference on computer vision*, pages 3119–3127, 2015.
- Hideyuki Tachibana, Katsuya Uenoyama, and Shunsuke Aihara. Efficiently trainable text-to-speech system based on deep convolutional networks with guided attention. In *2018 IEEE International Conference on Acoustics, Speech and Signal Processing (ICASSP)*, pages 4784–4788. IEEE, 2018.
- Heechul Jung, Min-Kook Choi, Jihun Jung, Jin-Hee Lee, Soon Kwon, and Woo Young Jung. Resnet-based vehicle classification and localization in traffic surveillance systems. In *Proceedings of the IEEE conference on computer vision and pattern recognition workshops*, pages 61–67, 2017.
- Dzmitry Bahdanau, Jan Chorowski, Dmitriy Serdyuk, Philemon Brakel, and Yoshua Bengio. End-to-end attention-based large vocabulary speech recognition. In *2016 IEEE international conference on acoustics, speech and signal processing (ICASSP)*, pages 4945–4949. IEEE, 2016.
- Yunpeng Chen, Haoqi Fan, Bing Xu, Zhicheng Yan, Yannis Kalantidis, Marcus Rohrbach, Shuicheng Yan, and Jiashi Feng. Drop an octave: Reducing spatial redundancy in convolutional neural networks with octave convolution. In *Proceedings of the IEEE/CVF International Conference on Computer Vision*, pages 3435–3444, 2019.
- Fazle Karim, Somshubra Majumdar, and Houshang Darabi. Insights into lstm fully convolutional networks for time series classification. *IEEE Access*, 7:67718–67725, 2019.

-
- Hoang Anh Dau, Anthony Bagnall, Kaveh Kamgar, Chin-Chia Michael Yeh, Yan Zhu, Shaghayegh Gharghabi, Chotirat Ann Ratanamahatana, and Eamonn Keogh. The ucr time series archive. *IEEE/CAA Journal of Automatica Sinica*, 6(6):1293–1305, 2019.
- Hassan Ismail Fawaz, Germain Forestier, Jonathan Weber, Lhassane Idoumghar, and Pierre-Alain Muller. Deep learning for time series classification: a review. *Data Mining and Knowledge Discovery*, 33(4):917–963, 2019.
- Angus Dempster, François Petitjean, and Geoffrey I Webb. Rocket: exceptionally fast and accurate time series classification using random convolutional kernels. *Data Mining and Knowledge Discovery*, 34(5):1454–1495, 2020.
- Jason Lines, Sarah Taylor, and Anthony Bagnall. Time series classification with hive-cote: The hierarchical vote collective of transformation-based ensembles. *ACM Transactions on Knowledge Discovery from Data*, 12(5), 2018.